X-ray Photoelectron Spectroscopy (XPS)

Yinan Liu, Tolga Atalay
Advanced Master Lab, SoSe 2022
Department of Physics, Freie Universität Berlin

Abstract

X-ray photoelectron spectroscopy (XPS) is a special form of photoelectron spectroscopy utilizing X-ray photons to liberate electrons form core levels of atoms and molecules into vacuum to probe electronic structures nondestructively. This well-established method is used to determine electronic structures by analyzing the kinetic energy of liberated electrons from surface of a sample. In this experiment, technical basis of X-ray photoelectron spectroscopy is investigated, and X-ray photoelectron spectroscopy is performed on several samples. We have successfully determined many characteristic structures in spectra, precisely located binding energies of orbitals, determined spin-orbit coupling constant for different orbitals, and determined composition of a coin and contaminants.

Theoretical Fundamentals

Photoelectric effect describes the emission of electron due photon and electron interaction. A photon with greater energy than binding energy of an electron can be absorbed to free electron from bound atom, if the liberated electron has enough energy (E_{kin}) to overcome work function (Φ) of the solid, the electron is emitted. Photoemission spectroscopy utilizes this phenomenon to measure binding energy of electrons bound to an atom or molecule.

Einstein's relation for photoelectron effect can be deduced from conservation of energy of incident photon, subject atom, and liberated electron:

$$E(A) + E_{photon} = E(A^*) + E_{kin} + \Phi$$
$$E_{kin} = E_{photon} - [E(A^*) - E(A)] - \Phi = E_{photon} - E_{Bind} - \Phi \quad (1)$$

Characteristic excitation processes in solids

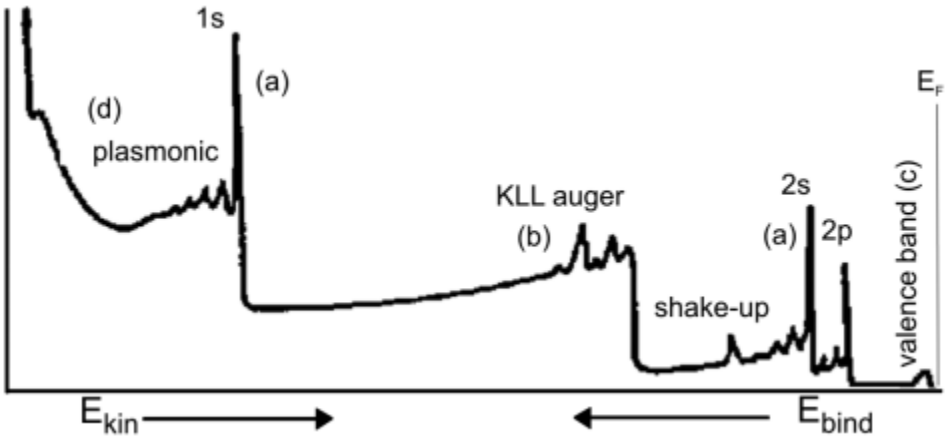

Figure 1. Overview of an XPS spectrum [1]

An overview of XPS spectrum shown in Fig 1, with characteristic peaks:

a) Emission from core levels
b) Auger Processes
c) Emission from the valence band
d) Secondary electron interactions in inelastic scattering

Shake-up lines from interactions with electrons and photoelectrons and satellite peaks by plasmon excitation in metals can also be observed.

Linewidth in photoemission
Linewidth in photoemission is affected by several factors such as characteristics of exciting X-ray, lifetime of states, interaction with phonons and resolution of analyzer.

Surface Sensitivity
XPS is highly surface sensitive due to photoelectrons having short mean free path. Figure 2 shows mean free path λ as a function of photoelectron energy with minimum mean free path between 10 eV and 100 eV. Photoelectron kinetic energy can be varied using different X-ray tube anode.

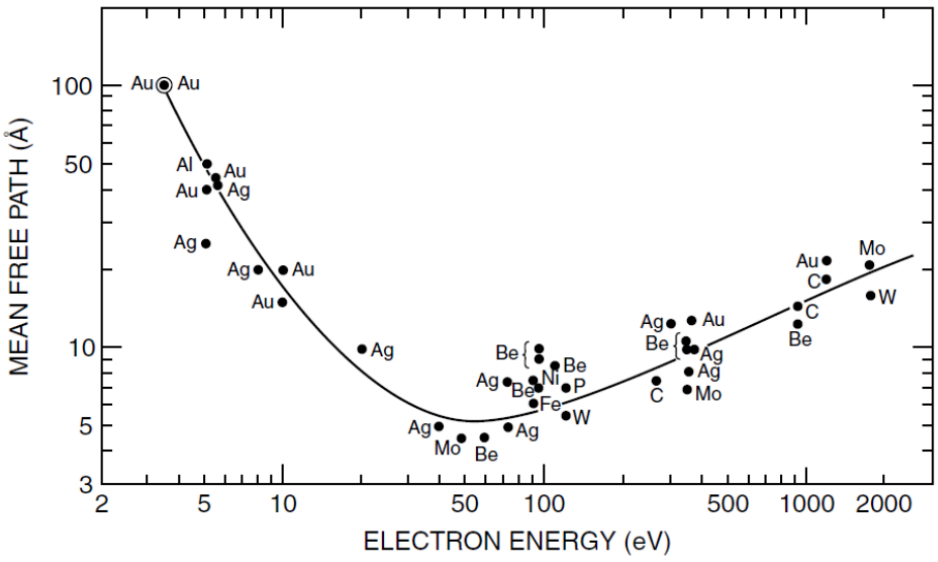

Figure 2. Mean free path and universal curve. [1]

Binding Energy

Binding energy is a function of many interactions:

$$E_B = E_B(atom) + \Delta E_{chem} + E_{mad} + E_{rel} \quad (2)$$

ΔE_{chem} is chemical shift due to neighboring atoms (Figure3).
ΔE_{mad} (Madelung constant) caused by electrostatic forces in the lattice.
ΔE_{rel} (Relaxation effects) describes many body effects.

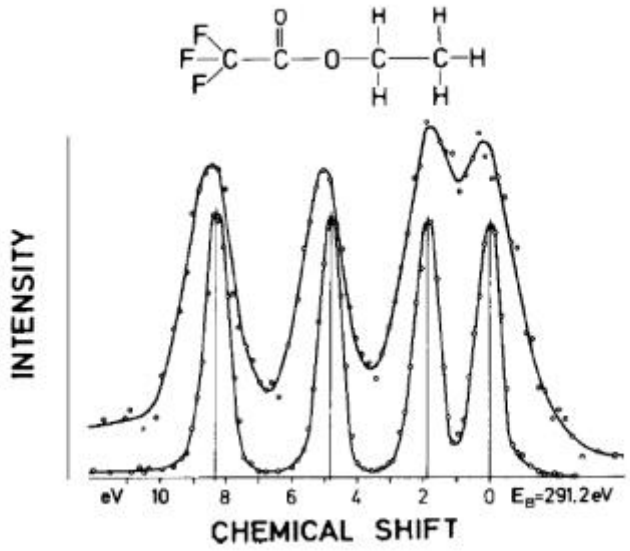

Figure 3. Chemical shifts of Chlorine in ethyl trifluoroacetate. [1]

Multiplet structures can be observed in XPS due to following interactions:

Spin Orbit Coupling

Spin-orbit interactions in full electron shell causes ground state to split into doublet with $\left(l+\frac{1}{2}\right) and\ \left(l-\frac{1}{2}\right)$ angular momentums. Shift in orbital energy due splitting is given by equation 3.

$$\Delta E = \frac{A(n,l)}{2}\big(j(j+1) - l(l+1) - s(s+1)\big) \quad (3)$$

Magnetic Spin-Spin exchange splitting

Energy splitting of a s-shell is caused by exchange coupling between full inner s-shell and magnetic spin moment of partially filled shell.

Experimental Set up

The experimental set up consists of a vacuum system, an X-ray source, an electron energy analyzer, an evaporator, and an O_2 dosing bottle. The vacuum system used in the experiment is an ultra-high vacuum (UHV) chamber, where the sample holder with our materials of interest is

held. The tested materials include sheet silver, and two sheets of steel for vapor deposition of Samarium, and a 10 Deutsche Mark coin.

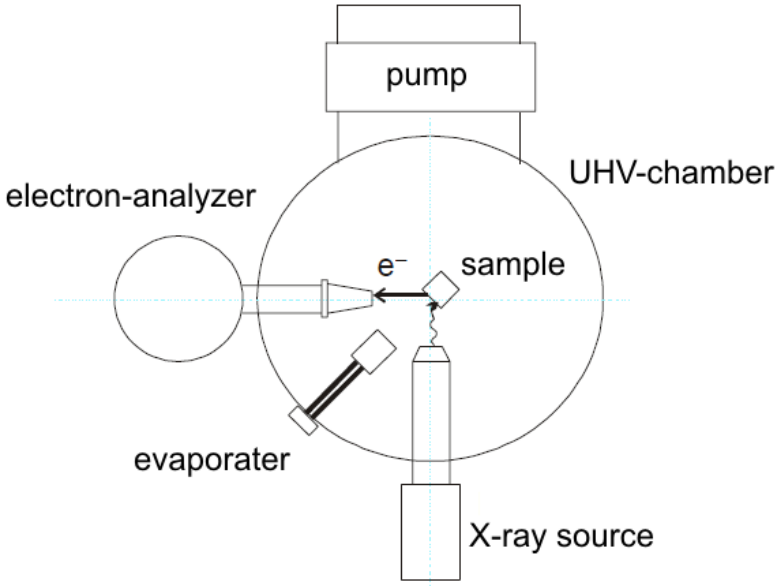

Figure 4. Schematics of an ultra-high vacuum chamber with photoemission equipment [1].

The UHV utilizes a turbo molecular pump which works well for heavy gases, but pumps light gases like H_2 with high particle speeds slowly. After reaching an initial pressure of 10^{-9} mbar, it is baked out for hours or up to days to get rid of residual water on the chamber's steel wall, until reaching final pressure of 10^{11} mbar.

The x-ray source consists of a cathode and an anode (Figure 5a). The cathode emits thermal electrons through heating (emission current 30mA), and is accelerated to the anode by a high voltage of 9kV to 12kV. The anode can be selected between Mg and Al for their characteristic emission spectrum (Figure 2).

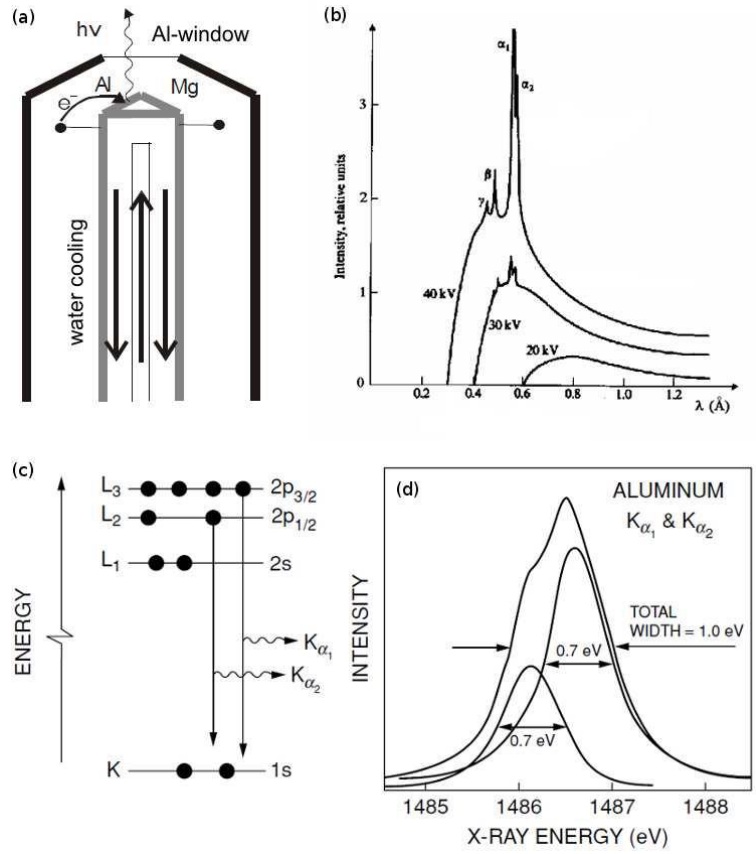

Figure 5. (a) Schematic structure of the double anode X-ray source. (b) Cu anode emission spectra. (c),(d) Al characteristic radiation [1].

The electron energy analyzer measures the kinetic energy of emitted photoelectrons. It consists of a hemi-spherical capacitor, and a channeltron as a detector. The hemi-spherical capacitor is made from electrical lens system with two metallic hemispheres (Figure 6). A pass voltage is applied to the hemispherical plates to reduce noise in the spectrum from low kinetic energy electrons in the secondary processes. The channeltron is made from a glass tube with high resistance material coated through and serves as a secondary electron multiplier.

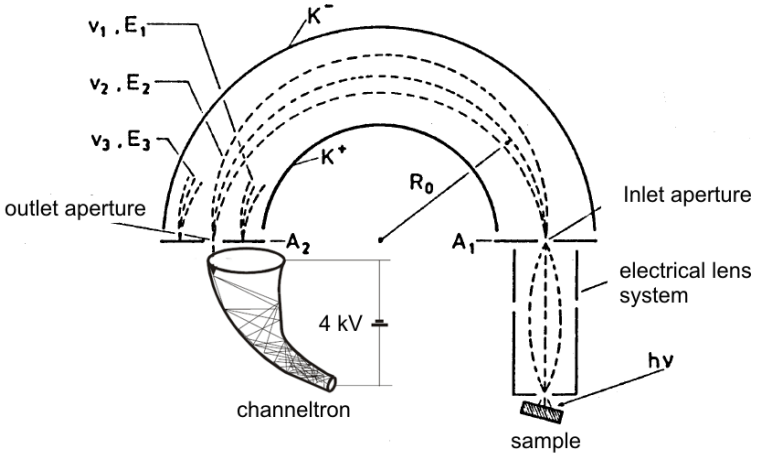

Figure 6. Schematics of the electron energy detector [1].

An evaporator is used to deposit the Samarium. It consists of a tantalum crucible, and a filament wrapped around it (Figure 4). Samarium will be stored and melted inside of the crucible that is heated up by current running through the filament.

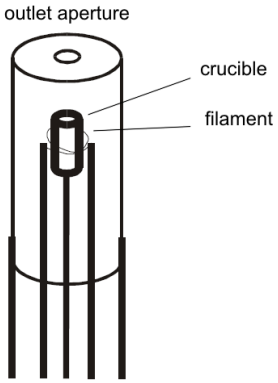

Figure 7. Schematics of the Samarium evaporator [1].

A bottle of oxygen that is connected to the leaking valve is used to dose the Sm surface in defined quantities. The unit used is Langmuir, which corresponds to the quantity when the surface is covered with a monolayer of dopant. It has the following relationship with SI units:

$$1\ Langmuir = 1torr * us = 1.33 * 10^{-6}\ mbar * s$$

Results

Spectra of a silver sample

Survey scan of the Ag Sample with magnesium x-ray source with 50eV pass energy is recorded and shown in figure 8 . Spectrum is shifted as reference binding energy to fermi level. Traces of oxygen and carbon are observed.

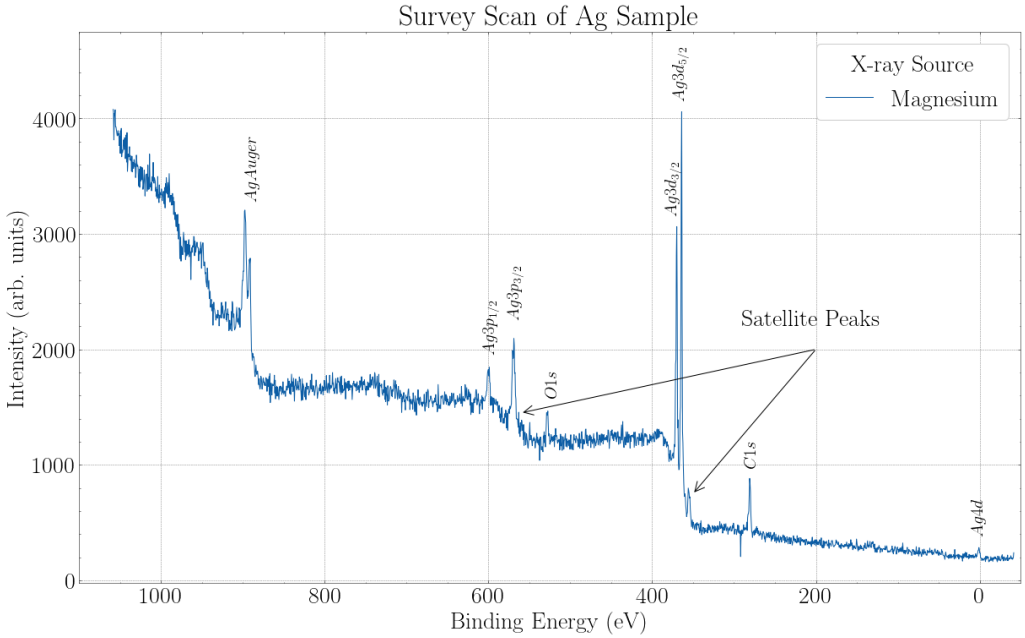

Figure 8. Overview spectra of Ag Sample, Mg anode.

Savitzky-Golay filter [2] is applied to remove noise and Tougaard [3]background subtraction is done to improve peak resolution as well as to obtain relative peak strengths. Figure 9 shows the post processed x-ray spectra of Ag sample.

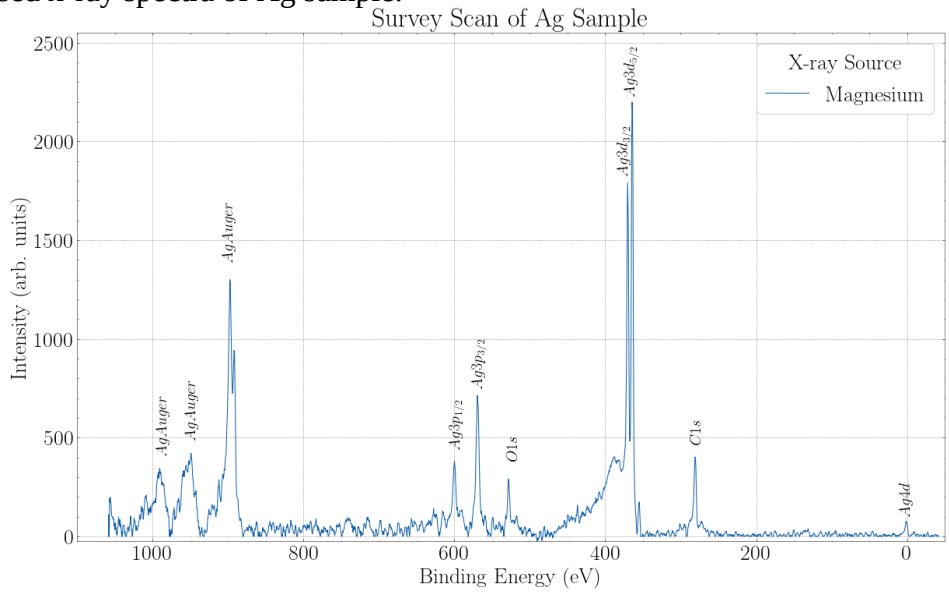

Figure 9. Post processed overview spectra of Ag Sample, Mg anode .

Another scan on the Ag sample accomplished by aluminum x-ray source and shown in figure 10.

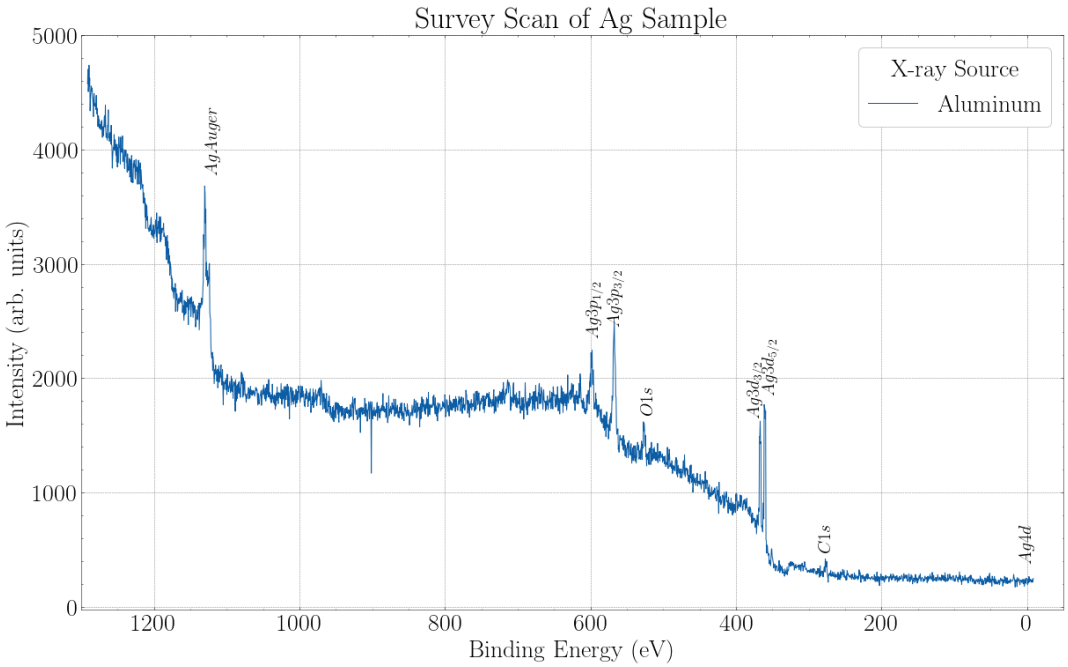

Figure 10. Overview spectra of Ag Sample, Al anode.

To distinguish Auger peaks, two spectra with different X-ray sources overlayed together as a function of photoelectron kinetic energy and shown in figure 11.

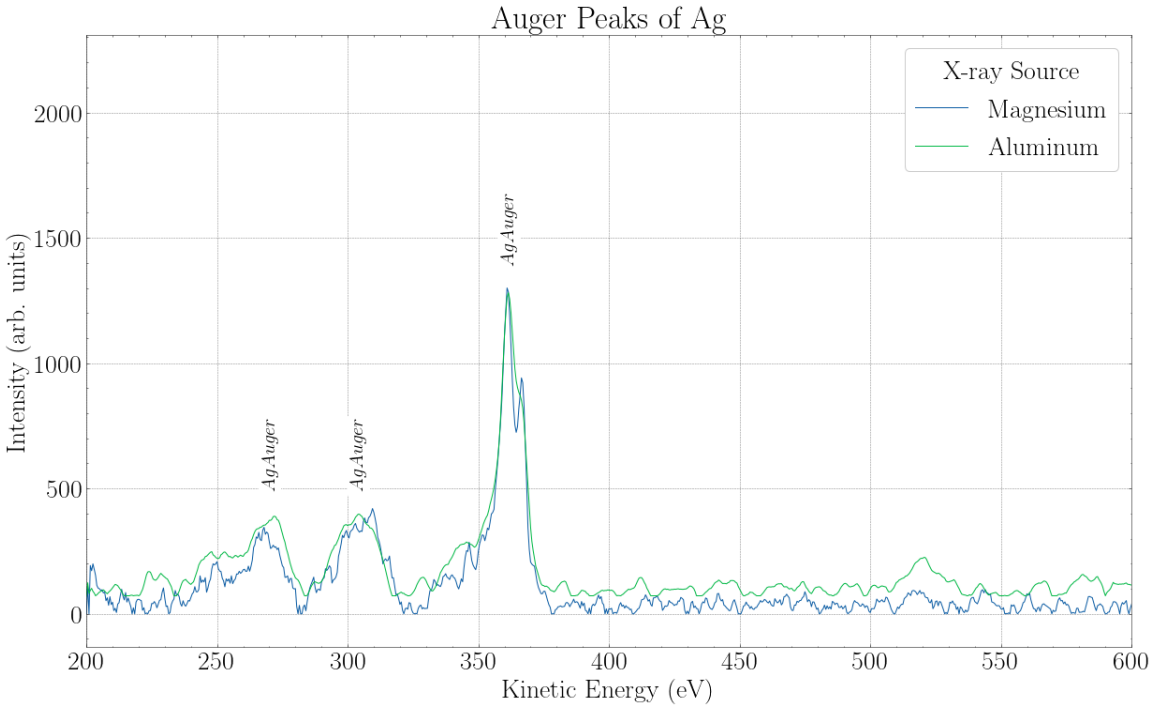

Figure 11. X-ray spectra of two different anodes showing Ag Auger peaks between 250eV and 400 eV Kinetic Energy.

Ag-3p Spectrum

Detailed scan of spin-orbit splitting in 3p peak of Ag is recorded as average of 5 individual scans. Savitzky-Golay filter is applied, and linear background is subtracted. Figures 12 and 13 shows 3p peaks with aluminum and magnesium x-ray sources respectively.

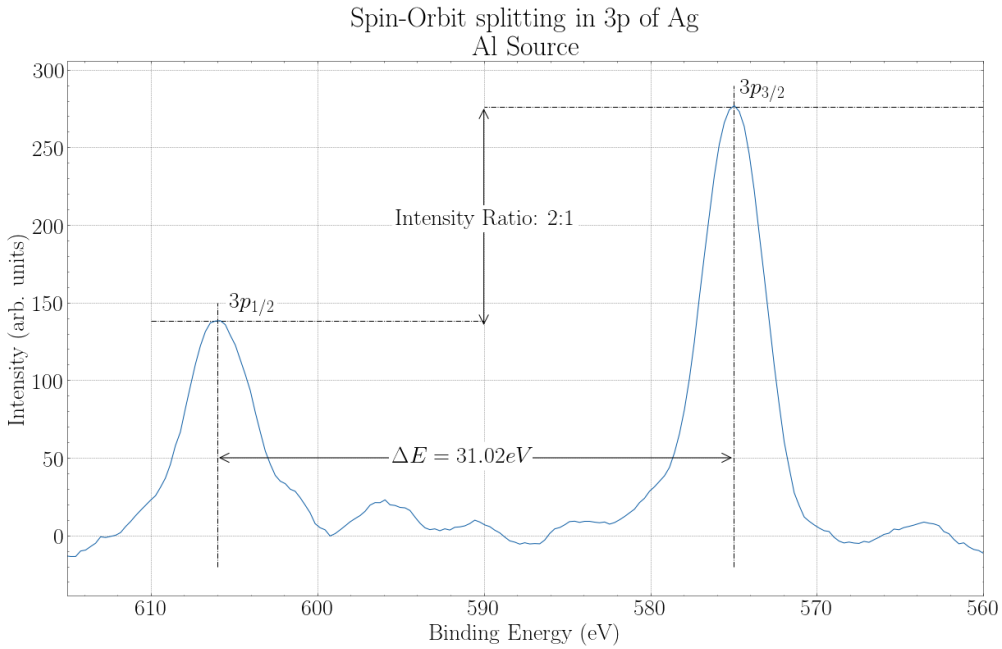

Figure 12. Spin-Orbit splitting in 3p of Ag, Al anode.

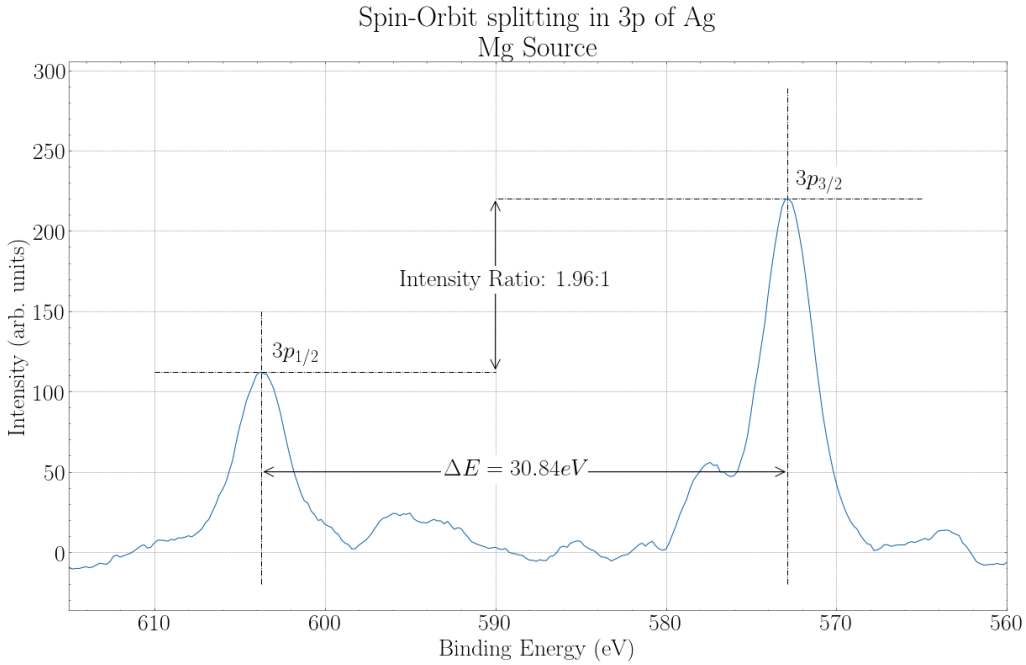

Figure 13. Spin-Orbit splitting in 3p of Ag, Mg Anode.

	Binding Energy (eV)		
State	*$Mg\ K\alpha$*	*$Al\ K\alpha$*	Literature
$3p_{3/2}$	573 ± 1	575 ± 1	573.0
$3p_{1/2}$	604 ± 1	606 ± 1	603.8

$$\langle H_{SO}\rangle_{njls} = \frac{A_{Ag}(n,l)}{2}[j(j+1) - l(l+1) - s(s+1)]$$

Splitting in 3p states into $3p_{3/2}$ and $3p_{1/2}$ has average energy difference of 31eV, Using the equation 3 we determine splitting constant $A(n,l)$:

$$\langle H_{SO}\rangle_{3P_{\frac{3}{2}}} - \langle H_{SO}\rangle_{3P_{\frac{1}{2}}} = \frac{A}{2}\left\{\left[\frac{3}{2}\left(\frac{3}{2}+1\right) - 1(1+1) - \frac{1}{2}\left(\frac{1}{2}+1\right)\right] - \left[\frac{1}{2}\left(\frac{1}{2}+1\right) - 1(1+1) - \frac{1}{2}\left(\frac{1}{2}+1\right)\right]\right\} = \frac{3}{2}A_{Ag}(3,1)$$

$$A_{Ag}(3,1) = 20.62 \pm 0.1ev$$

Ag-3d Spectrum

Splitting in 3d peak of Ag is investigated similarly as 3p peak. Figure 14 shows splitting in 3d peaks of the silver sample.

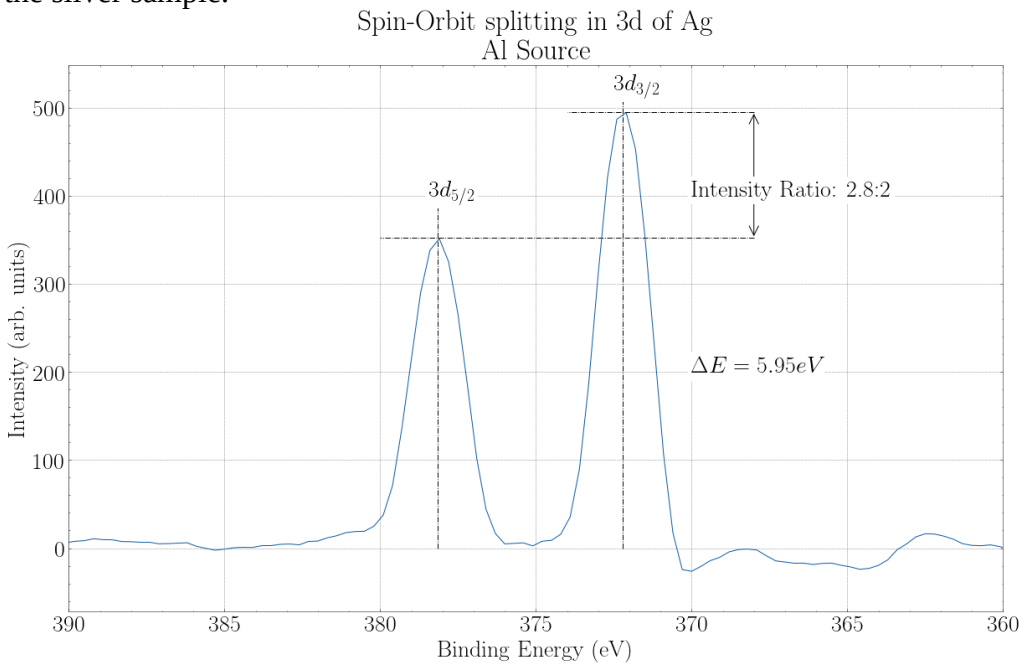

Figure 14. Spin-Orbit splitting in 3d of Ag, Al Anode.

	Binding Energy (eV)	
State	*Al Kα*	Literature
$3d_{5/2}$	372 ± 1	368.0
$3d_{3/2}$	378 ± 1	374.8

$$\langle H_{SO}\rangle_{3D_{\frac{5}{2}}} - \langle H_{SO}\rangle_{3D_{\frac{3}{2}}}$$
$$= \frac{A}{2}\left\{\left[\frac{5}{2}\left(\frac{7}{2}+1\right) - 2(2+1) - \frac{1}{2}\left(\frac{1}{2}+1\right)\right]\right.$$
$$\left. - \left[\frac{3}{2}\left(\frac{5}{2}+1\right) - 2(2+1) - \frac{1}{2}\left(\frac{1}{2}+1\right)\right]\right\} = \frac{5}{2}A_{Ag}(3,2)$$

$$A_{Ag}(3,2) = 2.38 \pm 0.1ev$$

Spectra of a samarium metal

Survey scans of the Sm sample are done with aluminum and magnesium x-ray sources. Similar to the method used to analyze the Ag sample is used to determine Auger peaks in the Sm sample. Figure 15 shows post-processed X-ray spectra of the Sm sample with Mg source.

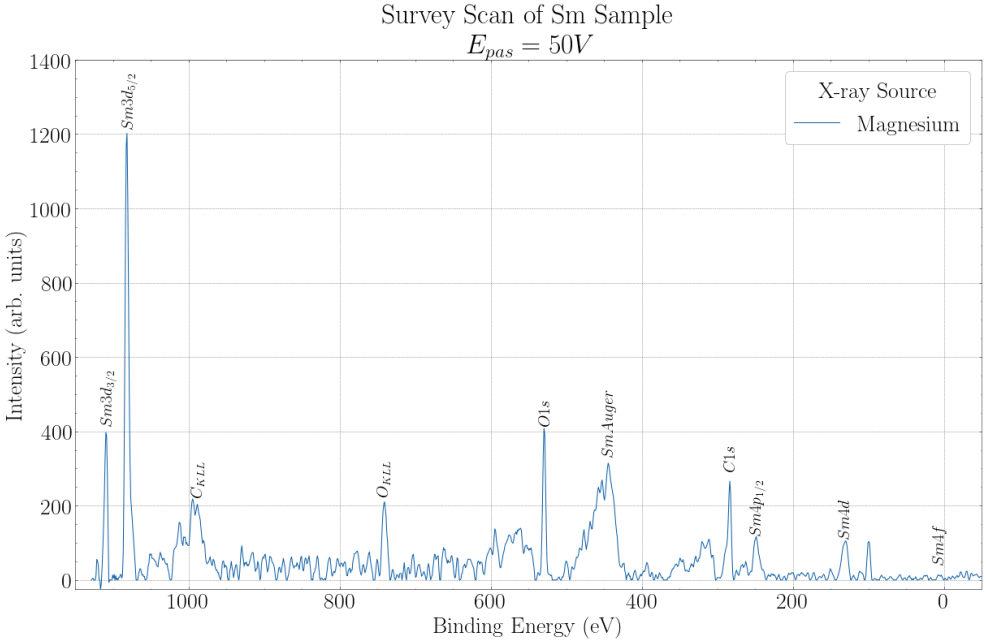

Figure 15. Post processed overview scan of Sm Sample, Mg Anode.

Traces of carbon and oxygen are also found in the Sm sample.

Sm-3d Spectrum

X-ray spectra showing spin-orbit splitting in 3d peak of the Sm sample is recorded as average of 5 individual scans. Savitzky-Golay filter is used, and Shirley background is subtracted. Figures 16 and 17 shows 3d peaks with 30V and 50V pass energies with Mg source.

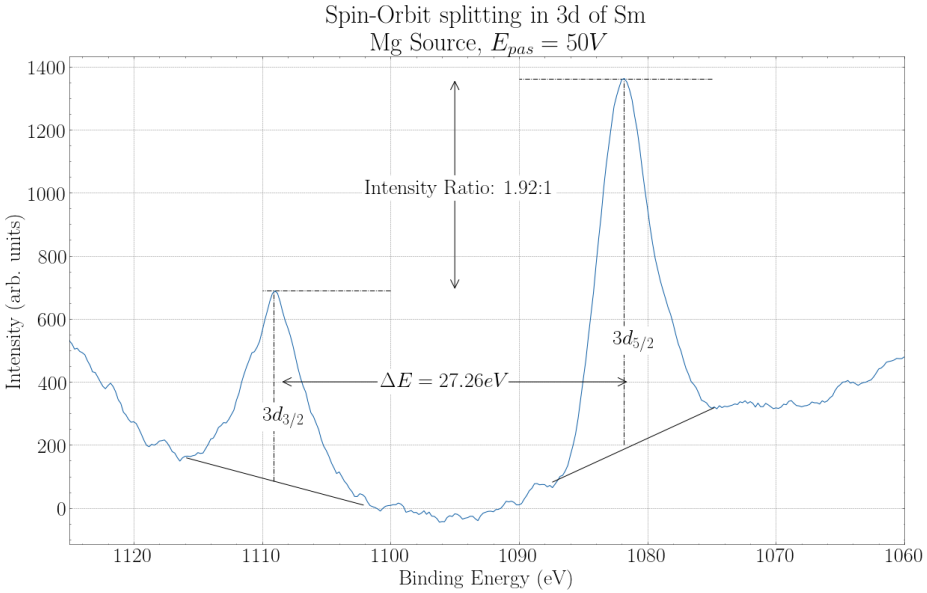

Figure 16. Spin-Orbit splitting in 3d of Sm, Mg Anode.

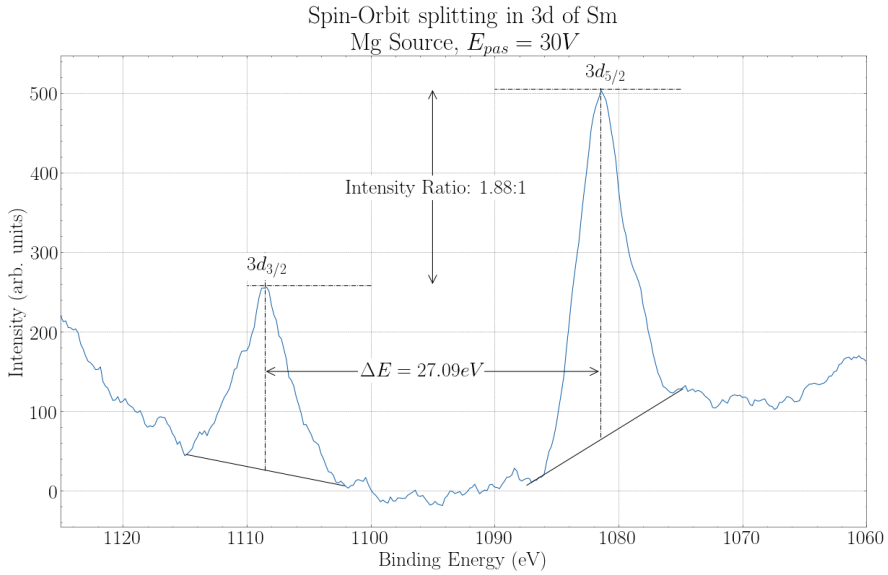

Figure 17. Spin-Orbit splitting in 3d of Sm, Mg Anode.

	Binding Energy (eV) $Mg\ K\alpha$		
State	30 eV	50 eV	Literature
$3d_{5/2}$	1108.6 ± 1	1109.1 ± 1	1110.9
$3d_{3/2}$	1081.5 ± 1	1082.9 ± 1	1083.4

$$\langle H_{SO}\rangle_{3D_{\frac{5}{2}}} - \langle H_{SO}\rangle_{3D_{\frac{3}{2}}} = \frac{A}{2}\left\{\left[\frac{5}{2}\left(\frac{5}{2}+1\right) - 2(2+1) - \frac{1}{2}\left(\frac{1}{2}+1\right)\right] - \left[\frac{3}{2}\left(\frac{3}{2}+1\right) - 2(2+1) - \frac{1}{2}\left(\frac{1}{2}+1\right)\right]\right\} = \frac{5A}{2}$$

$$A = 3.28 \pm 0.1ev$$

Fermi level and Sm 4f-spectrum of Samarium

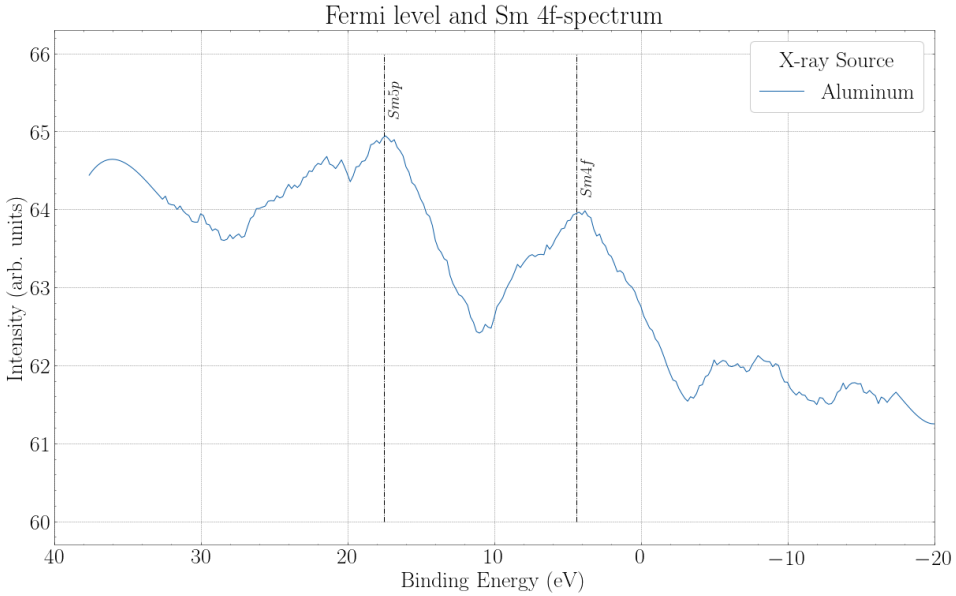

Figure 18. Fermi edge and 4f peaks of Sm, Al Anode.

	Binding Energy (eV)	
State	*Al Kα*	Literature
$Sm\ f_4$	4.4 ± 1	5.2
$Sm\ p_5$	17.5 ± 1	21.3

Coin

Survey scan of DM Coin shows the characteristic peaks of copper and silver metals. Presence of carbon, oxygen, and samarium are also noted.

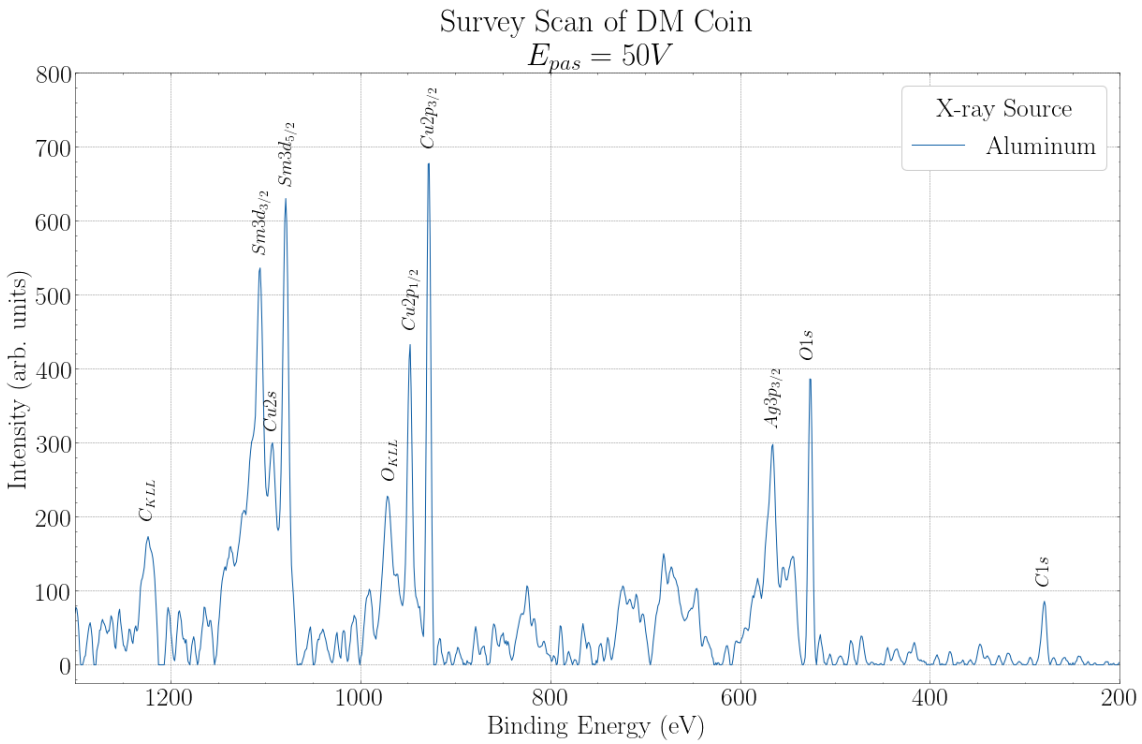

Figure 19. Overview scan of coin surface, Al Anode.

Discussion and Conclusion :
Overview scan of the silver sample clearly shows the characteristic Auger, 3d, 3p peak structures, fermi edge, satellite peaks and spin-orbit splitting of 3d and 3p peaks. Two unidentified peaks are then determined to be from Carbon and Oxygen contaminations. Applying digital filter and subtracting baseline greatly enhanced the peak structure resolution and allowed comparison of relative strengths of peak intensities. We determined the Auger peak positions by comparing two scans with different x-ray anodes. Auger peaks have the same photoelectron kinetic energy regardless of the anode material. One of the limiting factors in peak structure resolution is x-ray source, since it is impossible to resolve binding energies larger than source x-ray energy.

Splitting of 3p peaks in the silver sample are well defined, to decrease statistical fluctuations further we have averaged 5 individual scans and applied Savitzky-Golay filter. A linear baseline is subtracted to obtain relative intensity of the multiplets. Intensity ratio of $3p_{3/2}$ and $3p_{1/2}$ is close to expected ratio of 2:1 characteristic to splitting in principal orbital.
Peak positions of 3p peaks differ less than 1% than literature values.

A high-resolution spectrum of 3d peaks is obtained by scanning sample 5 times using aluminum and magnesium anodes. During the handling of data, scans with magnesium anode are lost. Splitting of 3d peaks in the silver sample are analyzed similarly as 3p peaks. Intensity ratio of $3d_{5/3}$ and $3d_{1/3}$ are determined to be 2.8:2, which is close to the expected ratio of 3:2 of splitting in d orbitals. Determined 3d peak positions differ by 1% from literature values.

In samarium overview scan we have observed the 3d, 4p, 4d, Auger peaks, traces of oxygen and carbon, and another unidentified peak with suspected silicon origin. Auger peaks are determined using the same technique used to determine Auger peaks in the silver sample.

5 scan average of 3d peaks region are obtained with aluminum anode for two different pass energies. Relative ratio of intensities of the 3d peaks determined to be 1.90:1 on average, which does not comparable to expected ratio of 3:2, one possible explanation for this discrepancy could be due to inadequate subtraction of Shirley background. Peak positions well-match the literature values. Pass energy reduces background noise by mainly eliminating photoelectrons from secondary processes. In this data we did not notice significant differences between spectra with 30V and 50V pass energies.

Fermi level of the samarium is determined by averaging 50 individual scans and applying Savitzky-Golay filter. Then spectrum is shifted to set reference of binding energy to fermi level. Although the spectrum resembled pure noise, averaging 50 different scans, and applying Savitzky-Golay filter revealed fermi level, 4f and 5p peaks. 15% and 18% errors in 4f and 5p peak positions respect to literature values calculated respectively.

An overview scan with Aluminum anode reveals peak structure with characteristic Copper, Silver, Samarium, Carbon, and Oxygen peaks by comparison with literature values [4], [5].X-ray spectra of the sample coin suggests this coin has a composition of copper and silver with surface contamination of samarium, oxygen, and carbon. While oxygen and carbon traces were found on the surfaces of all samples, samarium was not present on silver sample. Samarium presence on coin might have been caused by evaporation of samarium while coin was placed in samarium evaporator.

Reference:

[1] "X-ray Photoelectron Spectroscopy (XPS)." Freie Universitat, Department of Physics, May 16, 2011.

[2] Abraham. Savitzky and M. J. E. Golay, "Smoothing and Differentiation of Data by Simplified Least Squares Procedures.," *Anal. Chem.*, vol. 36, no. 8, pp. 1627–1639, Jul. 1964, doi: 10.1021/ac60214a047.

[3] S. Tougaard, "Formalism for quantitative surface analysis by electron spectroscopy," *J. Vac. Sci. Technol. Vac. Surf. Films*, vol. 8, no. 3, pp. 2197–2203, May 1990.

[4] Center for X-Ray Optics and Advanced Light Source, "X-Ray Data Booklet," *Tech. Electical Inf. Dep. - Lawrence Berkeley Natl. Lab. Berkeley*, 2001.

[5] John F. Mouler, W. F. Stickl, Peter E. Sobol, and K. D. Bomben, "Handbook of X-ray Photoelectron Spectroscopy," *ULVAC-PHI Inc 370 Enzo Chigasaki 235-8522 Jpn. Phys. Electron. USA Inc 18725 Lake Driv. East Chanhaussen Minn. 55317 USA.*